

Iron (II) impregnated double-shelled hollow mesoporous silica as acid-base bifunctional catalyst for the conversion of low-quality oil to methyl esters

Stefanus Kevin Suryajaya ^{a,1}, Yohanes Ricky Mulyono ^{a,1}, Shella Permatasari Santoso ^{a,b}, Maria Yuliana ^{a,*}, Alfin Kurniawan ^c, Aning Ayucitra ^a, Yueting Sun ^d, Sandy Budi Hartono ^a, Felycia Edi Soetaredjo ^{a,b}, Suryadi Ismadji ^{a,b}

^a Department of Chemical Engineering, Widya Mandala Catholic University Surabaya, Kalijudan 37, Surabaya, 60114, Indonesia

^b Department of Chemical Engineering, National Taiwan University of Science and Technology, 43, Keelung Rd., Sec. 4, Taipei, 10607, Taiwan

^c Department of Chemistry, National Sun Yat-Sen University, Kaohsiung, 80424, Taiwan

^d Department of Mechanical Engineering, University of Birmingham, Edgbaston, Birmingham, B15 2TT, United Kingdom

ARTICLE INFO

Article history:

Received 18 August 2020

Received in revised form

20 January 2021

Accepted 22 January 2021

Available online 25 January 2021

Keywords:

Bifunctional catalyst

Biodiesel

Renewable energy

Hollow mesoporous silica

Iron impregnation

Amine functionalization

ABSTRACT

To promote the use of low-quality oils in producing biodiesel, a bifunctional acid-base catalyst Fe/DS-HMS-NH₂ is fabricated using the two-step condensation technique. The obtained Fe/DS-HMS-NH₂ is of a doubled shell structure in spherical shape with a uniform size of 156 nm. Its hollow core (with a diameter of 86 nm) and two spatial shells with different active sites enables the esterification and transesterification reactions to be accomplished in a one-pot synthesis. The influences of four independent reaction variables on the yield of fatty acid methyl esters Y_F was studied, including catalyst loading m_c , reaction time t , reaction temperature T , and the methanol to degummed palm oil mass ratio $r_{m/o}$. The highest yield was obtained at 85.36% (w/w) when $m_c = 6\%$ (w/w), $t = 4.5$ h, $T = 60$ °C, and $r_{m/o} = 6:1$. The Fe/DS-HMS-NH₂ shows a good recyclability with $Y_F > 80\%$ (w/w) up to three reaction cycles.

© 2021 Elsevier Ltd. All rights reserved.

1. Introduction

The global fuel demand is growing rapidly as it undergoes an extensive urbanization. Our heavy reliance on fossil fuel brings the risk of unstable market price and reduced fuel availability. The gas emission from fossil fuel combustion also causes environmental concerns. Therefore, developing an alternative fuel that is biodegradable, sustainable and with a low carbon emission is the most significant energy and environmental challenge for us in the coming decades [1,2]. Since 2006, the Indonesian government has been committed to reducing carbon emissions by replacing fossil

fuels with biodiesel [3]. It is also declared that the use of biodiesel in diesel blend will be increased from B20 to B30 starting from 2020 [4], with a strategy to boost the domestic use of palm oil and lower down energy imports. Usually, biodiesel is obtained through the conventional transesterification process of refined oil [5]. However, the technologies of utilizing non-refined oil, specifically the low-quality oil, have currently attracted extensive interests and are being developed. Various types of low-quality oil have been studied to produce high-quality biodiesel using sundry of technical routes, including the two steps acidic esterification followed by basic transesterification [6], noncatalytic transesterification using alcohol under subcritical [7] and supercritical conditions [8], enzymatic transesterification [9] and solid-catalyzed transesterification [10]. Among the available routes, the use of heterogeneous (solid) catalysts has been attracting a growing interest in recent years, as it has the advantage of easier separation, tolerance to impurities (i.e., FFA, water and other minor compounds), and good reusability [11] which means minimal waste and toxic water

Abbreviations: FFA, Free fatty acids; FAME, Fatty acid methyl esters; DPO, Degummed palm oil; CPO, Crude palm oil; SS-HMS-NH₂, Single-shelled hollow mesoporous silica; DS-HMS-NH₂, Double-shelled hollow mesoporous silica; Fe/DS-HMS-NH₂, Iron (II) impregnated double-shelled hollow mesoporous silica.

* Corresponding author.

E-mail address: mariayuliana@ukwms.ac.id (M. Yuliana).

¹ These authors contributed equally to this work.

production [12] and environmentally friendly [13]. Boey et al. (2011) and Lam et al. (2010) also stated that heterogeneous catalysts lower the product contamination level, and reduce the corrosion problem [14,15]. Various solid catalysts and their modifications have been reported, such as zirconia [16], silica impregnated with zinc stearate (ZS/Si) [17], heterogeneous KF/ZnO catalyst [18], heterogeneous Zn/I₂ catalyst [12]. However, despite their insensitivity to impurities, these catalysts solely act as the mono functional catalysts, depending on their acidity nature and have the following disadvantages during the conversion of low-quality oil to biodiesel: (1) the reaction carried out in the presence of an acidic heterogeneous catalyst is slow, and at the same time, requires large amount of alcohol [19], meanwhile (2) the basic heterogeneous catalysts usually result in a lower biodiesel yield and purity, since this type of catalyst leaves the FFA unreacted during the reaction.

In this paper, we prepared and characterized a new class of heterogeneous catalyst, the double-shelled hollow mesoporous silica impregnated with divalent iron metal (Fe/DS-HMS-NH₂), to be used as an acid-base bifunctional catalyst in the production of biodiesel from a low-quality oil. This catalyst enables a simple process of converting low-quality oil to biodiesel by combining the two processes of esterification and transesterification into a single-stage process. This is achieved by having double active surface layers that facilitate the two reactions to run simultaneously. The primary (inner) shell is designed to promote the transesterification reaction by adding –NH₂ as the basic site, while the outer layer is impregnated with the divalent iron (Fe (II)), which is selected as the impregnated metals due to its nature as a strong Lewis acid, and its ability to change the oxidation level and activate the substance during the process [20].

The synthesis, characterization and catalytic activity of the Fe/DS-HMS-NH₂ will be investigated in this paper. Its performance as an acid-base bifunctional catalyst for biodiesel preparation will be examined at various conditions, including catalyst loading m_c (% w/w), reaction temperature T (°C), reaction time t (h), and the mass ratio of methanol to oil $r_{m/o}$. In this present research, degummed palm oil (DPO) is selected as the lipid material. With similar content of FFA and moisture as the crude palm oil (CPO), DPO is also classified as a low-quality oil, along with industrial fats, oils and greases, and other crude/waste lipids. Therefore, it is considered as a suitable raw material to determine the catalytic ability of Fe/DS-HMS-NH₂ in converting both FFA and triglycerides in DPO into biodiesel. We will also show that the Fe/DS-HMS-NH₂ can be regenerated and reused, which is regarded as an important feature for heterogeneous catalysts as it will reduce the cost for production and pollutant discharges [21,22]. The recyclability of the catalyst will be investigated at the operating condition giving the highest yield of fatty acid methyl esters (FAME) Y_F .

2. Materials and methods

2.1. Materials

CPO was collected from the local manufacturer in Indonesia. Prior to use, CPO was degummed using 1% (w/w) phosphoric acid (PA, 85% purity) at a temperature of 80–90 °C for 30 min to reduce the phosphorus content. Several important characteristics of the degummed CPO (i.e., DPO), namely free fatty acid content, acid value, saponification value, and moisture content were analyzed in accordance with the standard method of AOCS Ca 5a–40, Cd 3d–63, Cd 3d–25, and Ca 2e–84, respectively.

3-aminopropyl-triethoxysilane (APTES) was purchased from Fisher Scientific (Pittsburgh, USA), while other chemicals required for the fabrication of Fe/DS-HMS, namely iron (II) sulfate heptahydrate (FeSO₄·7H₂O, 99.99% purity), tetraethylorthosilicate

(TEOS), cetyltrimethylammonium bromide (CTAB), ethanol (98% purity), methanol (99.9% purity), hydrochloric acid (HCl, 37% purity), ammonium hydroxide solution (NH₄OH, 25% purity), and n-hexane (95% purity) were obtained from Merck (Merck, Germany). The FAMES standard (47885 U) containing 37 components FAME mix was procured from Supelco (Bellefonte, PA, USA). Ultra-high purity nitrogen gas (>99.0% purity) was purchased from Aneka Gas Industry Pty. Ltd., Indonesia. All chemicals used in this study were of analytical grade and required no further purification.

2.2. Preparation of DS-HMS-NH₂

In a typical synthesis, 0.14 g of CTAB, 20 ml of ethanol, 50 ml of deionized water and 1 ml of NH₄OH solution were simultaneously introduced into a glass beaker and mixed for 15 min at room temperature. Then 1 ml of TEOS was slowly added into the above solution and kept stirring for 24 h. The precipitates were collected through centrifugation at 4500 rpm for 30 min, triplicate ethanol washing, and drying at 120 °C overnight. After the calcination at 550 °C for 6 h, the single shelled hollow mesoporous silica (SS-HMS-NH₂) was obtained.

The outer shell of the particle was fabricated using a multilevel scheme based on SS-HMS-NH₂. In a typical synthesis, 0.5 g CTAB, 18 ml deionized water, and 50 ml of ethanol were introduced into a beaker glass. Meanwhile, 0.063 g of SS-HMS-NH₂ was added into a mixture of 4 ml deionized water and 8.5 ml of 25% (w/w) NH₄OH solution. The above two solutions were then combined and stirred for 15 min at 250 rpm, after which 100 μl TEOS and 21 μl APTES were slowly added into it and the mixture was kept stirring for 24 h to allow the condensation reaction of silica. Finally, the solid product was collected by centrifugation at 4500 rpm for 15 min, which was then repeatedly washed with 60 ml of ethanol and 4 ml of HCl, and oven-dried at 120 °C. The dried product was calcined at 550 °C for 6 h to obtain double-shelled hollow mesoporous silica (DS-HMS-NH₂).

2.3. Iron (II) impregnation onto DS-HMS-NH₂ surface

The impregnation of divalent iron onto the DS-HMS-NH₂ surface was achieved as follows to fabricate Fe/DS-HMS-NH₂ catalysts. In a typical synthesis, 0.1 g DS-HMS-NH₂ was mixed with 50 ml of deionized water under sonication for 30 min at room temperature. Meanwhile, two separate solutions were prepared: (1) 5 mg of FeSO₄·7H₂O was dissolved in 50 ml of deionized water, and (2) 0.2 g of CTAB was dissolved in 10 ml ethanol. Solution (1) and (2) were then added into the DS-HMS-NH₂ solution and stirred for 12 h at ambient conditions. The Fe/DS-HMS-NH₂ precipitates were separated by a centrifugation at 4500 rpm for 15 min, and then dried at 120 °C for 12 h and calcined at 550 °C for 5 h to obtain the Fe/DS-HMS-NH₂ powder.

2.4. Catalytic activity of Fe/DS-HMS-NH₂ at various reaction conditions

The *in-situ* esterification/transesterification reactions from DPO to FAME were carried out in a glass flask equipped with a reflux condenser and external heater under constant magnetic stirring (250 rpm) at various conditions. Specifically, the influence of four reaction parameters were investigated due to their relevance to industrial applications: catalyst loading m_c (% w/w), reaction temperature T (°C), reaction time t (h), and the mass ratio of methanol to DPO $r_{m/o}$. To determine the amount of Fe/DS-HMS-NH₂ catalyst that produces the maximum FAME yield Y_F , a few reactions were carried out with different amounts of Fe/DS-HMS-NH₂ ($m_c = 2\%, 4\%, 6\%, 8\%$, w/w) at the following condition: $T = 60$ °C,

$t = 4.5$ h and $r_{m/o} = 10:1$. Once the optimum catalyst loading is obtained, the catalytic activity of Fe/DS-HMS-NH₂ was investigated within an experimental matrix defined by $T = 40$ °C, 50 °C, 60 °C, $t = 0.5$ h, 2.5 h, 4.5 h, and $r_{m/o} = 2:1, 6:1, 10:1$. The experimental runs were designed in a random order using face centered-central composite design (CCF-CCD) as listed in Table 3. All the experimental runs were conducted with the same procedure.

After the reaction completed, Fe/DS-HMS-NH₂ catalyst was recovered by centrifugation at 4500 rpm for 15 min, and calcination at 550 °C for 5 h. The liquid product was subjected to a two-stage liquid-liquid extraction using methanol and n-hexane sequentially for purification. Then the FAME-rich phase was separated from the by-products (i.e., glycerol, excess methanol, soap, and the other unwanted materials) and evaporated under vacuum to obtain the final FAME product. As an evaluation of the catalytic activity of Fe/DS-HMS-NH₂, the yield of FAME was calculated by the following equation:

$$Y_F(\%, w/w) = \frac{m_F p_F}{m_s} \times 100 \quad (1)$$

where m_F is the mass of the final FAME product (g), p_F is the FAME purity (% w/w) obtained from equation (2) shown in the next section, and m_s is the total mass of the DPO (g).

2.5. Characterization of Fe/DS-HMS-NH₂ catalyst and FAME

The characterization of Fe/DS-HMS-NH₂ was conducted using field-emission scanning electron microscopy with energy dispersive X-Ray spectroscopy (FESEM/EDX), transmission electron microscopy (TEM), nitrogen sorption, and thermogravimetric analysis (TGA). The FESEM/EDX images were taken on a JEOL JSM-6500 F (Jeol Ltd., Japan) running at 15 kV with a working distance of 12.4 mm, while TEM was carried out on JEOL JEM-2100 with an accelerating voltage of 200 kV. Nitrogen sorption analysis was conducted at 77 K on a Micrometrics ASAP 2010 Sorption Analyzer. The sample was degassed at 423 K prior to analysis. To determine the thermal stability and volatile component fraction of the Fe/DS-HMS-NH₂ catalyst, a TGA analysis was performed using TG/DTA Diamond instrument (Perkin-Elmer, Japan).

The final FAME product characteristics, including its kinematic viscosity (at 40 °C), flashpoint, cetane number, acid value and calorific value were determined according to the standard methods of ASTM D445, ASTM D93, ASTM D613, ASTM D664, and ASTM D240, respectively. The purity of FAME (p_F) in the final product was analyzed using a gas chromatograph (Shimadzu GC-2014) equipped with a split/splitless injector and a flame ionization detector (FID). The stationary phase used for separation was the narrow bore non-polar DB-WAX column (30 m × 0.25 mm ID × 0.25 μm film thickness, Agilent Technology, CA), and the temperature profile for the analysis was in accordance with the study conducted by Harjijaya et al. (2019) [23]. Methyl heptadecanoate (MH) was used as an internal standard, while an external FAME reference (47885 U, containing 37 components FAME standard mix) was used to obtain the FAME compositional profile. p_F is calculated by the following equation:

Table 1
Textural properties of Fe/DS-HMS-NH₂.

Material	S_{BET} (cm ² /g)	Pore volume (cm ³ /g)	Pore size (nm)
Fe/DS-HMS-NH ₂	782.84	0.64	2.43

Table 2
Characteristics of DPO.

Parameter	Value
FFA (% w/w)	5.54
Moisture Content (% w/w)	0.20
Saponification Value (mg KOH/g DPO)	234.08
Acid Value (mg KOH/g DPO)	12.04
Molecular weight (g/mol)	756.62

Table 3
Experimental matrix at the optimum catalyst loading $m_c = 6\%$ (w/w).

Run	Input Parameters			Y_F (% w/w)
	T (°C)	t (h)	$r_{m/o}$	
1	60	4.5	10:1	85.24 ± 1.19
2	40	0.5	10:1	40.27 ± 0.58
3	40	2.5	6:1	55.09 ± 0.76
4	50	4.5	6:1	75.15 ± 0.65
5	50	2.5	10:1	60.07 ± 0.44
6	40	0.5	2:1	35.19 ± 0.92
7	40	4.5	10:1	70.22 ± 1.01
8	50	2.5	2:1	67.03 ± 0.51
9	60	4.5	2:1	80.11 ± 0.68
10	50	2.5	6:1	65.16 ± 0.47
11	50	2.5	6:1	66.96 ± 0.73
12	50	2.5	6:1	65.87 ± 0.79
13	50	0.5	6:1	65.01 ± 0.37
14	60	4.5	6:1	85.36 ± 0.62
15	50	2.5	6:1	63.21 ± 0.42
16	60	0.5	10:1	70.01 ± 0.56
17	50	2.5	6:1	63.20 ± 0.69
18	50	2.5	6:1	67.18 ± 0.45
19	60	0.5	2:1	69.09 ± 0.53
20	40	4.5	2:1	59.11 ± 0.78

$$p_F(\%, w/w) = \left(\frac{\sum A_F - A_{MH}}{A_{MH}} \right) \left(\frac{V_{MH} C_{MH}}{m_F} \right) \times 100 \quad (2)$$

where $\sum A_F$ is the total peak area of FAME, A_{MH} is the corresponding area of methyl heptadecanoate (MH) peak, V_{MH} is the volume of MH solution (ml), C_{MH} is the actual concentration of MH solution (g/ml), and m_F is the actual mass of the final FAME product (g).

2.6. Recyclability of Fe/DS-HMS-NH₂

Fe/DS-HMS-NH₂ was repeatedly used for the transesterification process at the operating condition where the maximum yield of FAME was obtained. The recyclability of Fe/DS-HMS-NH₂ was determined by the number of repetitions until when the yield became lower than 80% (w/w). The purity and yield of FAME were analyzed according to the procedures in section 2.4–2.5. All experiments were carried out in triplicates to verify the results.

3. Result and discussions

3.1. The mechanism scheme of Fe/DS-HMS-NH₂ fabrication

The Fe/DS-HMS-NH₂ was synthesized by a two-step co-condensation technique. The mechanism scheme in Fig. 1 illustrates the fabrication route: (1) firstly, TEOS and CTAB undergo a co-condensation reaction along with the ammonium solution; (2) then CTAB, the soft template of the core, is removed by calcination, and the SS-HMS-NH₂ is thus formed; (3) TEOS, APTES, and CTAB undergo another co-condensation reaction on the outer surface of the SS-HMS-NH₂ spheres; (4) DS-HMS-NH₂ nanosphere is obtained by removing CTAB and APTES in calcination; (5) the divalent iron (Fe

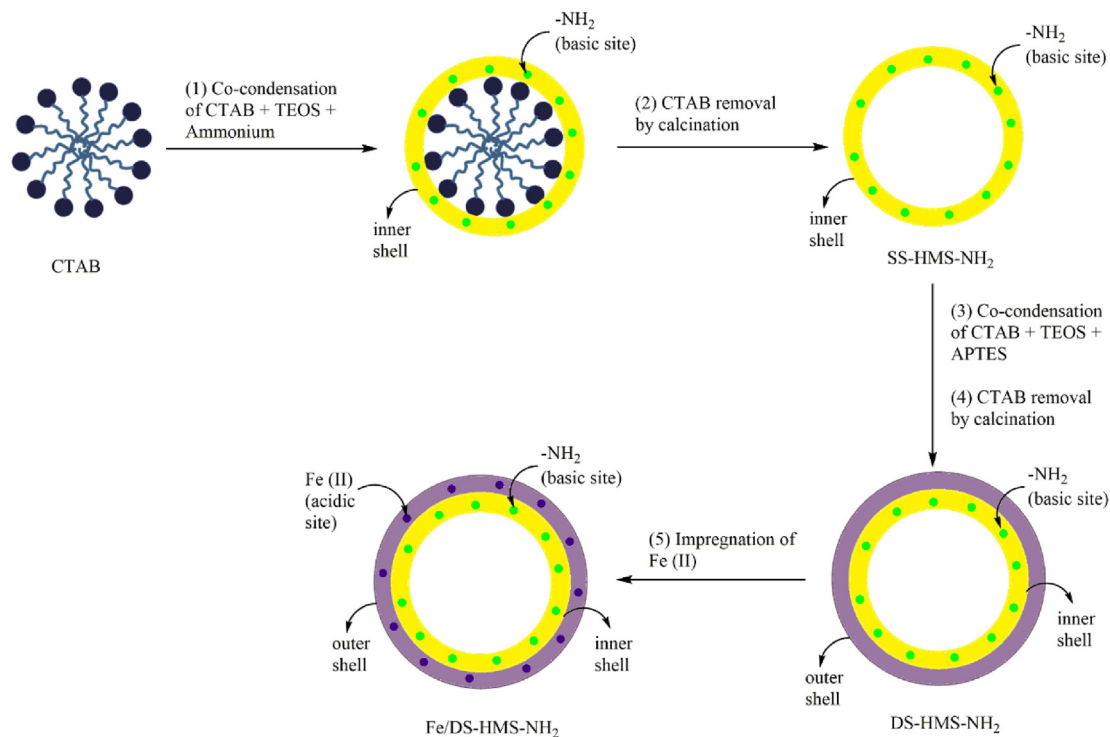


Fig. 1. The mechanism scheme of Fe/DS-HMS-NH₂ fabrication.

(II)) was incorporated onto the surface of DS-HMS-NH₂ by a traditional wet impregnation technique, and the Fe/DS-HMS-NH₂ nanosphere is obtained.

3.2. Characterization of Fe/DS-HMS-NH₂ catalysts

Fig. 2a, c–d present the SEM and TEM images of the Fe/DS-HMS-

NH₂ catalyst synthesized by the co-condensation technique. The catalyst is spherical with a uniform size at ca. 156 nm (Fig. 2a). Notably, Fe/DS-HMS-NH₂ is composed of two shell layers, indicated by the darker color of the inner shell in Fig. 2c and d. Its hollow-core structure is clearly presented with the diameter of 86 nm (Fig. 2d). The shell thicknesses of the inner and outer layer of Fe/DS-HMS-NH₂, are 22 nm and 13 nm, respectively. The impregnation of Fe (II)

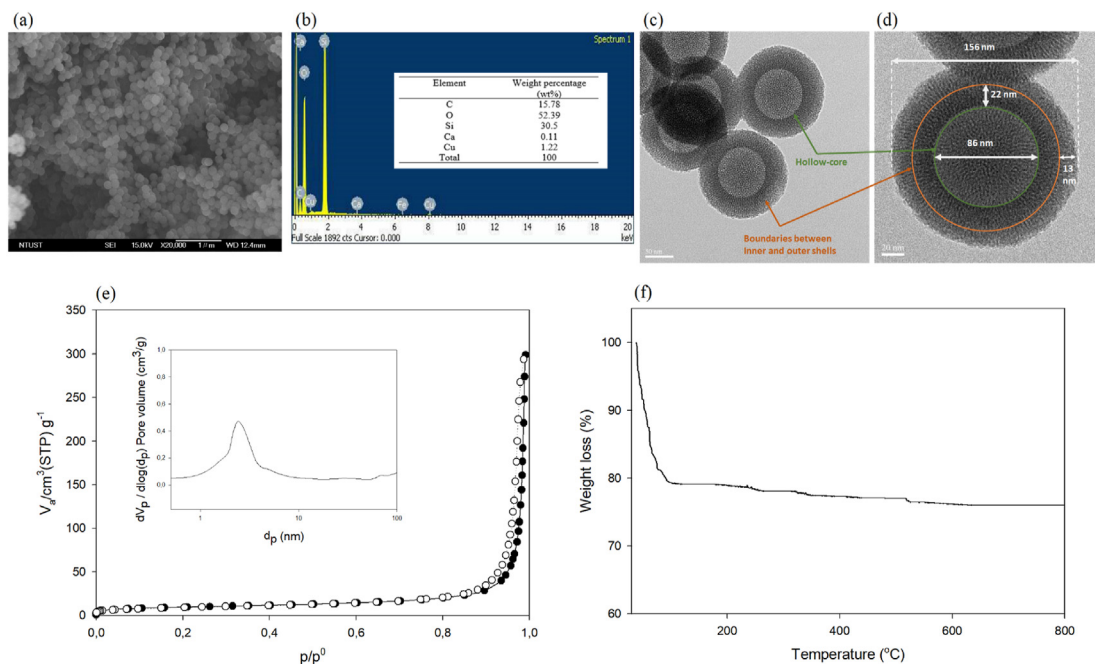


Fig. 2. (a) SEM image, (b) Elemental composition, (c)–(d) TEM images at various magnifications, (c) BJH pore size distribution curve, (e) Nitrogen adsorption-desorption isotherm with BJH pore size distribution curve (inset), (f) Thermogravimetric profile of the Fe/DS-HMS-NH₂ catalyst.

on the surface of the silica layer was successful, evidenced from the EDX result showing a percentage of 2.87% (Fig. 2b). Based on the fabrication procedure, it was reasonable to consider that the Fe (II) sites and basic amino sites were spatially isolated and located in different shells.

The textural properties of Fe/DS-HMS-NH₂ analyzed by the nitrogen sorption are presented in Table 1 and Fig. 2e. The nitrogen adsorption and desorption isotherm of the catalyst exhibits a typical type-IV isotherm, indicating the presence of a mesoporous structure with worm-like capillary pores molded by the CTAB micelles. The pore size of the mesoporous structure is found to be 2.43 nm (Fig. 2e (inset)). A steep increase of the nitrogen adsorption amount at p/p^0 close to unity also suggests that there are macropores structure within the particle, corresponding to the hollow core. Similar adsorption and desorption profile also pointed out that the pores are highly accessible. The specific surface area S_{BET} obtained in this study was 782.84 m²/g, lower than the value 1100–1350 m²/g for a similar double shelled hollow mesoporous silica [22]. Such a discrepancy was likely due to the reason that it was strongly influenced by the shell thickness. Zhou et al. (2014) reported that when the thickness of hollow mesoporous silica nanoparticles (HMSN) increases from 46 nm to 82 nm, the surface area of HMSN particles was declined from 986 m²/g to 614 m²/g [24]. Zhou et al. (2014) and Cao et al. (2011) also observed that an increase in the particle mass due to the addition of TEOS and CTAB in the synthesis of the second shell lowers the surface area, since the amount of TEOS during the fabrication is directly proportional to the thickness of the shell [24,25]. Meanwhile, the pore volume of Fe/DS-HMS-NH₂ (0.64 cm³/g) was found to be slightly higher than that reported by You et al. (2018) (0.61 cm³/g) [22]. Based on its textural analysis, Fe/DS-HMS-NH₂ possesses comparable specific surface area and pore volume with those of existing heterogeneous catalysts (i.e., HMS-Al@MS-NH₂ [22], char-based catalyst [26], γ -alumina industrial-grade catalyst [27], and copper-based metal-organic framework [28]), which usually range from 200 to 1300 cm²/g and 0.18–1.68 cm³/g respectively.

To demonstrate the feasibility of Fe/DS-HMS-NH₂ for the reactions at an elevated temperature, its thermal stability was investigated. The TGA profile in Fig. 2f shows a 20% decrease in weight up to the temperature of 100 °C, attributed to the removal of free moisture content. Further heating up to 800 °C does not significantly decrease the mass of Fe/DS-HMS-NH₂, suggesting that the catalyst is stable at high temperatures [29]. Therefore, our Fe/DS-HMS-NH₂ can be considered as a promising heterogeneous catalyst for the *in-situ* esterification/transesterification reaction.

3.3. The catalytic activity of Fe/DS-HMS-NH₂ in the *in-situ* esterification/transesterification of DPO

The characteristics of DPO as the raw material for biodiesel preparation are presented in Table 2. As homogenous catalysts are sensitive to impurities, the conversion of DPO to FAME for biodiesel production usually requires two reaction steps, namely acid-catalyzed esterification to lower the FFA content by converting them into FAME, and basic catalyzed transesterification to convert the acyl glycerides into FAME. However, heterogeneous catalysts can have good tolerance towards the FFA and water content in the lipid materials [10]; for Fe/DS-HMS-NH₂, its two spatial shells with different active sites can facilitate the above two reactions in a one-pot process, and therefore efficient conversion from DPO to FAME is achieved in a single step.

Fig. 3 presents the FAME yield obtained at various Fe/DS-HMS-NH₂ loadings at the condition of $T = 60$ °C, $t = 4.5$ h and $r_{\text{m/o}} = 10:1$. The results indicate that the yield of FAME is proportional to the number of active sites offered by the Fe/DS-HMS-NH₂ [30,31];

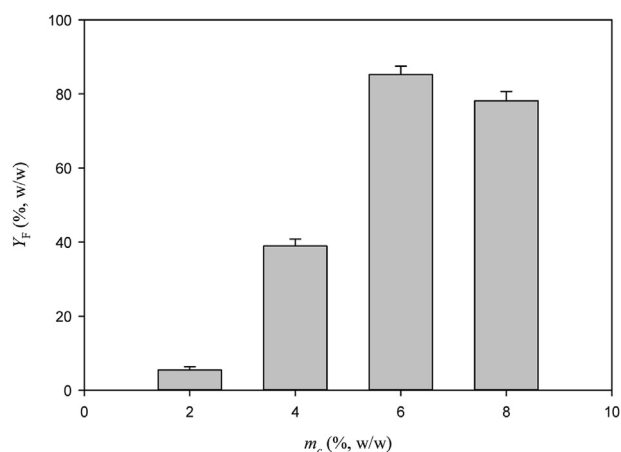


Fig. 3. The yield of FAME at various Fe/DS-HMS-NH₂ loadings with the reaction condition of $T = 60$ °C, $t = 4.5$ h and $r_{\text{m/o}} = 10:1$.

therefore Y_F increases with m_c when the latter is within 6% (w/w). This agrees well with previous work on biodiesel production using different solid catalysts, e.g., pomacea sp. shell-based CaO [30], sulfonated biochar [31], and KI/mesoporous silica [32]. A maximum yield 85.24% (w/w) is obtained when the catalyst loading $m_c = 6\%$ (w/w). Further increase of the Fe/DS-HMS-NH₂ results in a reduced yield of FAME, which is probably due to the aggregation and inconsistent dispersity of the catalyst in the reaction system of an enhanced viscosity [33,34]. Cai et al. (2018) and Samart et al. (2010) also mentioned that excess catalyst may also disturbed the mixing between the reactants, due to stronger adsorption of the reactants to the catalyst [35,36].

At a constant catalyst loading $m_c = 6\%$ (w/w), Fig. 4 and Table 3 present the FAME yield Y_F at various reaction time t , temperature T , and mass ratio of methanol to DPO $r_{\text{m/o}}$. The maximum $Y_F = 85.36\%$ (w/w) (with a purity of 97.89% (w/w)) is obtained at the condition of $T = 60$ °C, $t = 4.5$ h, $r_{\text{m/o}} = 6:1$. Based on the experimental results, the reaction time t was the most significant factor, followed by $r_{\text{m/o}}$ and T , which is supported by the Pareto chart of the standardized effect in Fig. 5 showing that t , $r_{\text{m/o}}$, and the two-way interaction between t and T are the three significant parameters in the reaction system.

The effect of reaction temperature on the production of biodiesel using Fe/DS-HMS-NH₂ is shown in Fig. 4a and b. An increased reaction temperature contributes to a higher yield, with the maximum achieved at 60 °C, which is related to the fact that both esterification and transesterification reaction are endothermic and reversible [38,39]. At a higher reaction temperature, the kinetic energy and mobility of reactant molecules increase, promoting the collisions between the molecules and Fe/DS-HMS-NH₂ particles which then increases the reaction rate constant and shift the reaction towards the product [38,40]. Moreover, the mass transfer of the reactant molecules through the boundary layer of Fe/DS-HMS-NH₂ is also accelerated at an elevated temperature, resulting in the faster diffusion of the reactants into the pore of catalyst; hence, improving the FAME yield.

Specifically, Fig. 4a and c shows a significant increase of the FAME yield by extending the duration of the biodiesel synthesis from 0.5 h to 4.5 h, at a constant temperature or mass ratio of methanol to DPO. Longer reaction time provides sufficient time for the reactants to reach the active sites of Fe/DS-HMS-NH₂ through adsorption and diffusion, and convert DPO into FAME [41]. Meanwhile, prolonged duration of reaction also gives the catalyst more time to adsorb the reactant and desorb the reaction product [28].

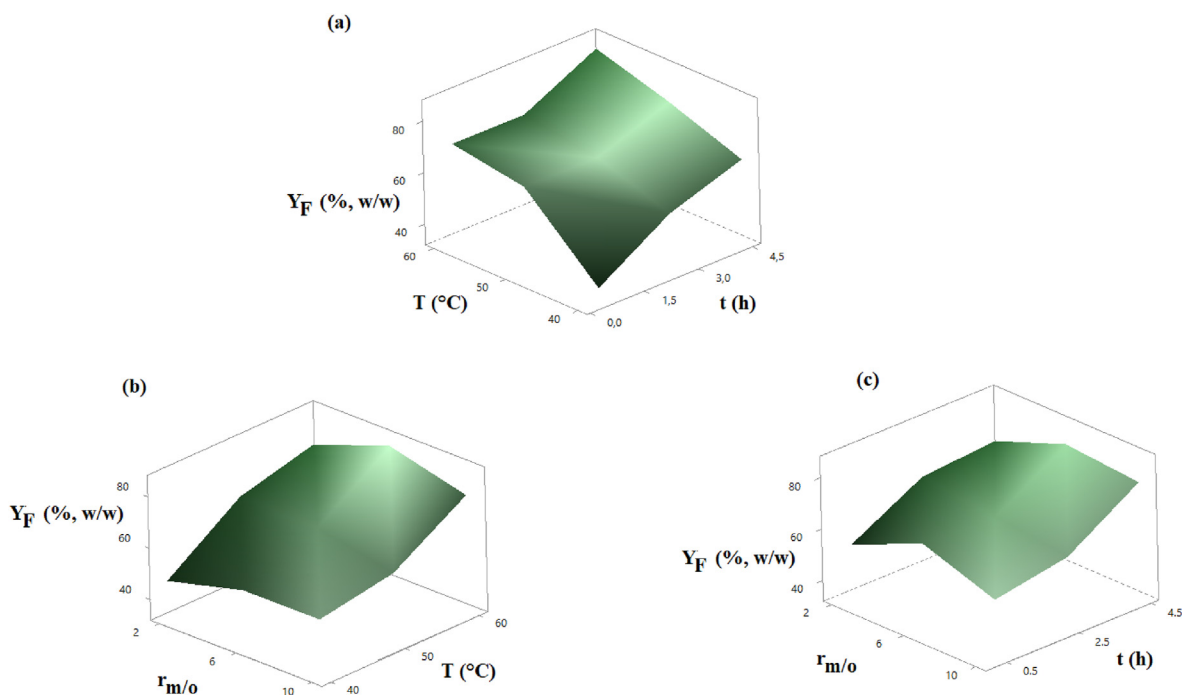


Fig. 4. The FAME yield Y_F (% w/w) at various (a) T and t , (b) T and $r_{m/o}$, and (c) t and $r_{m/o}$.

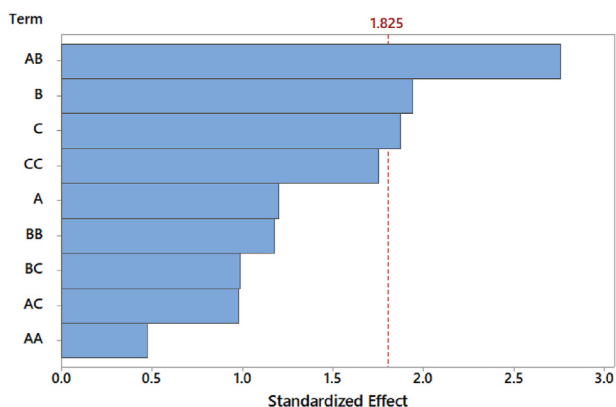


Fig. 5. Pareto chart of the standardized effect for the biodiesel preparation with Fe/DS-HMS-NH₂, using Y_F as the response at a 95% confidence interval where $A = T$, $B = t$, $C = r_{m/o}$.

Wei et al. (2009) also mentioned that adsorption and desorption of reactants from the catalyst is the rate-determining step in the overall reaction [42]. Therefore, allowing longer contact between the reactant molecules and the catalyst ensures high conversions of FFA and acyl glycerides to FAME.

Stoichiometrically, 3 mol of methanol are required to react with 1 mol of triglycerides in the transesterification reaction, while 1 mol of methanol is needed to react with 1 mol of free fatty acids in the esterification reaction [43,44]. Both reactions are known to be reversible; thus, the amount of methanol in the two reactions is usually provided in excess to shift the reaction equilibrium to the product side. As seen from Fig. 4b and c, having excess methanol from $r_{m/o} = 2:1$ to $r_{m/o} = 6:1$ contributes to a higher FAME yield, while further addition up to $r_{m/o} = 10:1$ has no improvement. While most studies agree that excess methanol is desirable to allow more frequent interactions between the lipid and methanol triggering the formation of FAME, Pangestu et al. (2019) found that excess

methanol may also accelerate the production of glycerol despite the higher yield of FAME [28]. As the esterification and transesterification are both reversible, a higher concentration of glycerol in the reaction system may induce a reverse reaction to the reactant side, creating an equilibrium between the products and reactants [28]. Hayyan et al. (2011) also reported that an excessive amount of methanol causes higher solubility of glycerol in the FAME phase that could lead to a complicated separation between biodiesel and glycerol [45]. Moreover, from the techno-economic viewpoint, the higher mass ratio of methanol to DPO also increases the material and processing cost [23,45]. Therefore, it can be concluded that the optimum level is $r_{m/o} = 6:1$.

A comparison of the FAME yield produced using Fe/DS-HMS-NH₂ with other existing catalysts is given in Table 4. It is notable that although the value of Y_F is higher when the refined feedstock is used as the reactant, the reaction time and the mass ratio of methanol to oil used in this study are lower. Moreover, among the studies using low-quality oil as raw lipid material, Fe/DS-HMS-NH₂ shows a higher catalytic activity compared with the other catalysts reported by Omar and Amin (2011), and Bala et al. (2017). This shows that Fe/DS-HMS-NH₂, as a bifunctional catalyst, is able to enhance the yield of biodiesel at a comparable operating condition, which is due to its ability to convert not only triglycerides but also FFA into FAME in a one-pot system. The analysis result of the final FAME product shows that the conversion of FFA after reaction reaches 95.6%.

The fuel properties of the final FAME product are presented in Table 5. The measurement results indicate that the product resulted in this study has comparable combustion and flow properties with those of the commercial biodiesel. The calorific value (45.143 MJ/kg) is also within the range required in the common petrodiesel (42–46 MJ/kg).

Meanwhile, its compositional profile is obtained by comparing the methyl ester peaks in the chromatogram with those in the external FAME standard (47885 U, containing 37 components FAME standard mix). The 12 identified peaks are 3.05% myristoleic acid

Table 4
The comparison of catalytic activity of several heterogeneous catalysts for biodiesel production.

Catalyst	Reactants	Operating condition	Yield (%)	References
Mesoporous zinc-doped silica	Cyanoacetate ester	$T = 60\text{ }^{\circ}\text{C}$, $t = 24\text{ h}$, $r_{m/o} = 10:1$, $m_c = 7\%$ (w/w)	94.0	[17]
Alumina-supported KI	Refined soybean oil	$t = 8\text{ h}$, $r_{m/o} = 15:1$, $m_c = 2.5\%$ (w/w)	96.0	[37]
Sr/ZrO ₂	Waste cooking oil	$T = 115.5\text{ }^{\circ}\text{C}$, $t = 169\text{ min}$, $r_{m/o} = 29:1$ (mol/mol), $m_c = 2.7\%$ (w/w)	79.7	[16]
Phosphotungstic acid-loaded KIT-5	Waste cooking oil	$T = 70\text{ }^{\circ}\text{C}$, $t = 4\text{ h}$, $r_{m/o} = 2:1$ (v/v), $m_c = 26.5\%$ (w/w)	83	[21]
Fe/DS-HMS-NH ₂	DPO	$T = 60\text{ }^{\circ}\text{C}$, $t = 4.5\text{ h}$, $r_{m/o} = 6:1$ (v/v), $m_c = 6\%$ (w/w)	85.36	This study

Table 5
Fuel properties of the final FAME product.

Properties	Methods	Unit	Final FAME product	ASTM D6751
Kinematic viscosity (at 40 °C)	ASTM D445	mm ² /s	2.64	1.9–6.0
Flashpoint	ASTM D93	°C	164.2	93 min
Cetane number	ASTM D613	–	55.7	47 min
Acid value	ASTM D664	mg KOH/g	0.24	0.5 max
Calorific value	ASTM D240	MJ/kg	45.143	–

methyl ester (C14:1), 2.37% cis-10-pentadecanoic acid methyl ester (C15:1), 35.78% palmitic acid methyl ester (C16:0), 8.13% palmitoleic acid methyl ester (C16:1), 8.36% stearic acid methyl ester (C18:0), 32.57% oleic acid methyl ester (C18:1n9c), 3.05% elaidic acid methyl ester (C18:1n9t), 1.17% cis-8,11,14-eicosatrienoic acid methyl ester (C20:3n6), 2.48% arachidonic acid methyl ester (C20:4n6), 0.52% cis-5,8,11,14,17-eicosapentaenoic acid methyl ester (C20:5n3), 1.07% erucic acid methyl ester (C22:1n9), 1.45% cis-13,16-docosadienoic acid methyl ester (C22:2).

3.4. Recyclability of Fe/DS-HMS-NH₂

An important feature of using heterogeneous catalysts for biodiesel preparation is its recyclability. In order to determine the recyclability of Fe/DS-HMS-NH₂, several reaction cycles were conducted in series using the operating condition of $m_c = 6\%$ (w/w), $T = 60\text{ }^{\circ}\text{C}$, $t = 4.5\text{ h}$, $r_{m/o} = 6:1$. Fe/DS-HMS-NH₂ was recovered following the method described in section 2.4, while fresh methanol and DPO were used in every cycle. The catalytic ability of the recycled Fe/DS-HMS-NH₂ for *in-situ* esterification/trans-esterification process is presented in Fig. 6. The result indicates that recycled Fe/DS-HMS-NH₂ can maintain a high yield of FAME above 80% (w/w) until the third cycle, close to the yield of fresh catalyst 85.36% (w/w). The purity of FAME for the first three cycles are 97.89%, 97.66% and 98.01% (w/w) respectively, higher than the

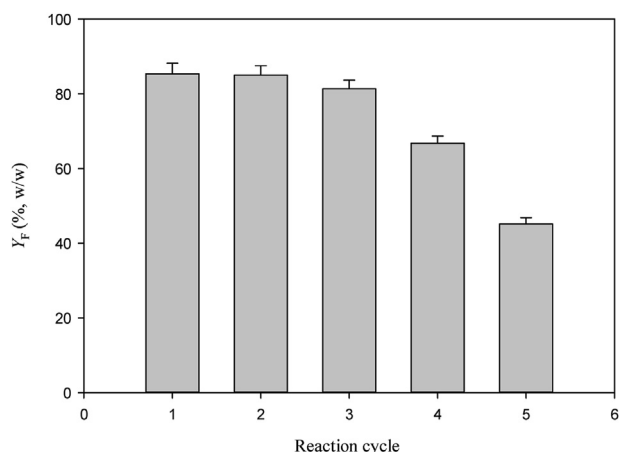


Fig. 6. Recyclability of Fe/DS-HMS-NH₂ in the *in-situ* esterification/trans-esterification of DPO.

commercial purity (96.5%, w/w). These results indicate that the catalytic activity of Fe/DS-HMS-NH₂ is maintained at a high level after regeneration. A significant drop in catalytic ability is observed from the fourth cycle in Fig. 6; similar performance has been reported for some other heterogeneous catalysts where three cycles seem to be an average number in term of their recyclability [46,47]. The catalytic deactivation of Fe/DS-HMS-NH₂ is generally due to the pore blockage caused by the contact between active sites on the catalyst surface and the deactivation-induced components, namely free glycerol, acyl glycerides, and biodiesel. Moreover, the high content of FFA in DPO also plays an important role in the deactivation of Fe/DS-HMS-NH₂ catalyst because FFA tends to neutralize the basic sites in the inner shell of Fe/DS-HMS-NH₂ [48], resulting in the generation of amine-carboxylate that induces the formation of emulsion.

3.5. The reaction mechanism of the *in-situ* esterification/trans-esterification of DPO using Fe/DS-HMS-NH₂

In the preparation of biodiesel from DPO, Fe/DS-HMS-NH₂ acts as both acid and base catalysts to facilitate the esterification of FFA and the transesterification of acyl glycerides. The main steps for the reaction mechanism catalyzed by Fe/DS-HMS-NH₂ are the formation of nucleophilic alkoxides, the nucleophilic attack on the electrophilic part of the carbonyl group of the triglycerides, and electron delocalization [49,50] as depicted in Fig. 7. The detailed description is as follows:

Step 1: Acyl glycerides, FFA and methanol enter the surface of catalyst through the adsorption process to reach the outer shell impregnated by the divalent iron. In this step, FFA undergoes the electron delocalization to form a carbocation and a carbanion, where the latter binds to the iron embedded on the catalyst.

Step 2: The reaction continues as the methoxide anion of methanol attacks the carbocation, whereas the hydronium cation attaches to the hydroxyl group of FFA to form water.

Step 3: Through the electron delocalization of the carbon atom, the water is released from the complex with FAME and the iron-embedded catalyst, followed by the release of FAME from the catalyst.

Step 4: The reaction continues when the acyl glycerides and methanol diffuse further to the amine-functionalized inner shell. The oxygen atom in the carbonyl group of acyl glycerides readily binds to the amine active sites.

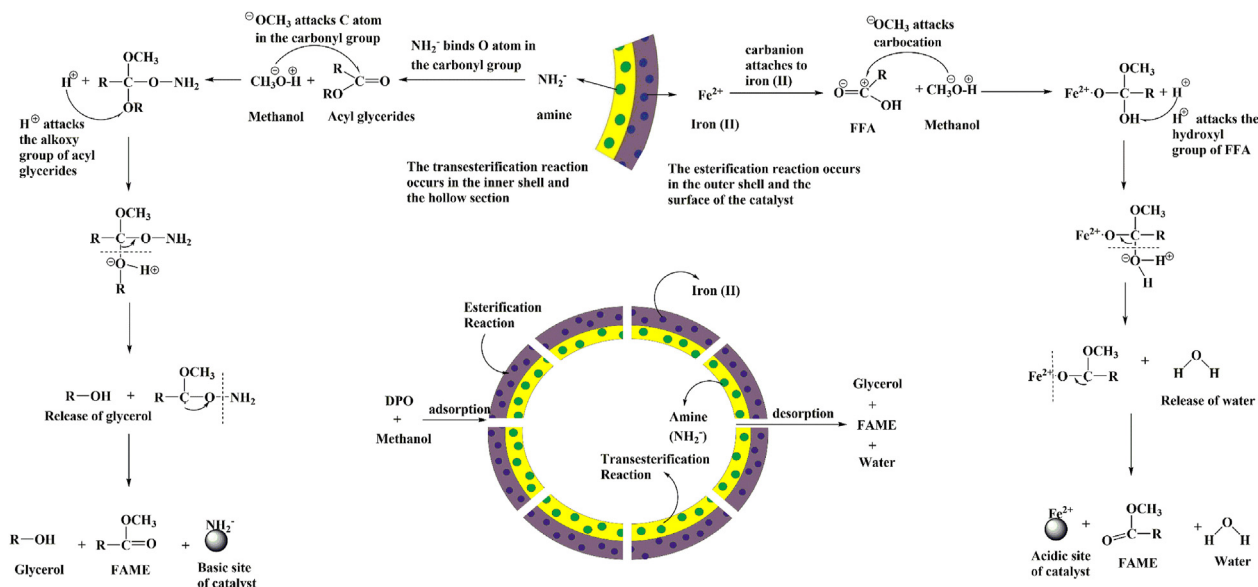


Fig. 7. The reaction mechanism of the *in-situ* esterification/transesterification of DPO using Fe/DS-HMS-NH₂.

Step 5: Subsequently, the methoxide anion of the methanol attacks the carbon atom in the carbonyl group of acyl glycerides, while the protonated H⁺ binds to the alkoxy group (RO⁻) of the acyl glycerides to form a complex of amine-functionalized catalyst with FAME and glycerol.

Step 6: Again, through the delocalization of oxygen in the complex, the glycerol and amine-functionalized catalyst are successively released from the complex.

Step 7: All three products, including FAME, glycerol, and water are then desorbed to the surface of the Fe/DS-HMS-NH₂ catalyst.

4. Conclusions

Fe/DS-HMS-NH₂ is synthesized through the two-step condensation technique and successfully employed as a heterogeneous catalyst for preparing biodiesel from DPO, a lipid source with significant FFA and moisture content. The obtained Fe/DS-HMS-NH₂ has a uniform spherical shape with a particle size of 156 nm and hollow diameter of 86 nm. It is composed of two spatial silica shells with different active sites, and their thickness are 22 nm for the inner shell and 13 nm for the outer shell. Fe/DS-HMS-NH₂ has a specific surface area of 782.84 m²/g with a pore volume of 0.64 cm³/g, comparable with the existing solid catalysts. In the *in-situ* esterification/transesterification process using the Fe/DS-HMS-NH₂ catalyst, reaction time *t* is the variable with most significant influence on the yield of FAME *Y_F*, followed by the reaction temperature *T* and the mass ratio of methanol to DPO *r_{m/o}*. The maximum *Y_F* is 85.36% (w/w), obtained at the following conditions: *T* = 60 °C, *t* = 4.5 h, and *r_{m/o}* = 6:1, with a catalyst loading of 6% (w/w). Notably, Fe/DS-HMS-NH₂ catalyst shows a good recyclability, with the yield staying above 80% for three reaction cycles. Therefore, Fe/DS-HMS-NH₂ is a promising heterogeneous catalyst to obtain biodiesel from DPO or other lipid materials with high FFA and water content. Further study on (1) the extension of the catalyst lifetime by creating a technique suitable for its regeneration, and also (2) the design of a plausible route between the current research and its industrial application should be the main focus for future research expansion.

CRedit authorship contribution statement

Stefanus Kevin Suryajaya: Conceptualization, Methodology, Investigation, Software, Writing - original draft. **Yohanes Ricky Mulyono:** Conceptualization, Methodology, Investigation, Software, Writing - original draft. **Shella Permatasari Santoso:** Conceptualization, Data curation, Supervision. **Maria Yuliana:** Conceptualization, Resources, Visualization, Writing - review & editing, Supervision. **Alfin Kurniawan:** Investigation, Resources. **Aning Ayucitra:** Investigation, Validation. **Yueting Sun:** Writing - review & editing. **Sandy Budi Hartono:** Software, Validation. **Felycia Edi Soetaredjo:** Resources, Visualization. **Suryadi Ismadji:** Resources, Validation.

Declaration of competing interest

The authors declare that they have no known competing financial interests or personal relationships that could have appeared to influence the work reported in this paper.

Acknowledgments

The authors acknowledge the funding supports from Widya Mandala Catholic University Surabaya and World Class Research Program, Indonesian Ministry of Research and Technology, through the research grant no. 2263/WM01/N/2020 and 130B/WM01.5/N/2020, respectively. We also thank Professor Chun-Hu Chen, National Sun Yat Sen University, and Taiwan Tech (National Taiwan University of Science and Technology) for providing the facility for the catalyst characterizations.

References

- [1] P. Agung, D. Hartono, A.A. Awirya, Pengaruh Urbanisasi Terhadap Konsumsi Energi Dan Emisi CO₂: analisis Provinsi di Indonesia (The Effect of Urbanization on Energy Consumption and CO₂ Emissions: an Analysis of Provinces in Indonesia), J. Ekon. Kuantitatif Terap. 1 (2017) 9–17, <https://doi.org/10.24843/jekt.2017.v10.i01.p02>.
- [2] A. Fitriyatus, A. Fauzi, B. Juanda, Prediction of Fuel supply and consumption in Indonesia with system dynamics model, J. Ekon. Dan Pembang. Indones. 17 (2018) 118–137.

- [3] F.T.R. Silalahi, T.M. Simatupang, M.P. Siallagan, Biodiesel produced from palm oil in Indonesia: current status and opportunities, *AIMS Energy* 8 (2020) 81–101, <https://doi.org/10.3934/energy.2020.1.81>.
- [4] F. Nangoy, B.C. Munthe, Indonesia President Wants B30 in Use by Jan 2020: Cabinet Secretary, Reuters, 2019.
- [5] J.M. Marchetti, A summary of the available technologies for biodiesel production based on a comparison of different feedstock's properties, *Process Saf. Environ. Protect.* 90 (2012) 157–163, <https://doi.org/10.1016/j.psep.2011.06.010>.
- [6] K. Suwannakarn, E. Lotero, K. Ngaosuwan, J.G. Goodwin Jr., Simultaneous free fatty acid esterification and triglyceride transesterification using a solid acid catalyst with in situ removal of water and unreacted methanol, *Ind. Eng. Chem. Res.* 48 (2009) 2810–2818, <https://doi.org/10.1021/ie800889w>.
- [7] Y.A. Tsigie, L.H. Huynh, S. Ismadji, A.M. Engida, Y.H. Ju, In situ biodiesel production from wet *Chlorella vulgaris* under subcritical condition, *Chem. Eng. J.* 213 (2012) 104–108, <https://doi.org/10.1016/j.cej.2012.09.112>.
- [8] P.D. Patil, V.G. Gude, A. Mannarswamy, P. Cooke, N. Nirmalakhandan, P. Lammers, S. Deng, Comparison of direct transesterification of algal biomass under supercritical methanol and microwave irradiation conditions, *Fuel* 97 (2012) 822–831, <https://doi.org/10.1016/j.fuel.2012.02.037>.
- [9] A. Kumari, P. Mahapatra, V.K. Garlapati, R. Banerjee, Enzymatic transesterification of *Jatropha* oil, *Biotechnol. Biofuels* 2 (2009) 1, <https://doi.org/10.1186/1754-6834-2-1>.
- [10] R. Mat, R.A. Samsudin, M. Mohamed, A. Johari, Solid catalysts and their application in biodiesel production, *Bull. Chem. React. Eng. Catal.* 7 (2012) 142–149, <https://doi.org/10.9767/bcrec.7.2.3047.142-149>.
- [11] W. Suryaputra, I. Winata, N. Indraswati, S. Ismadji, Waste capiz (*Amusium cristatum*) shell as a new heterogeneous catalyst for biodiesel production, *Renew. Energy* 50 (2013) 795–799, <https://doi.org/10.1016/j.renene.2012.08.060>.
- [12] H. Li, W. Xie, Transesterification of soybean oil to biodiesel with Zn/II catalyst, *Catal. Lett.* 107 (2006) 25–30, <https://doi.org/10.1007/s10562-005-9727-9>.
- [13] A.A. Refaat, A.A. Refaat, Archive of SID Different techniques for the production of biodiesel from waste vegetable oil, *Int. J. Environ. Sci. Tech.* 7 (2010) 183–213.
- [14] P.L. Boey, G.P. Maniam, S.A. Hamid, Performance of calcium oxide as a heterogeneous catalyst in biodiesel production: a review, *Chem. Eng. J.* 168 (2011) 15–22, <https://doi.org/10.1016/j.cej.2011.01.009>.
- [15] M.K. Lam, K.T. Lee, A.R. Mohamed, Homogeneous, heterogeneous and enzymatic catalysis for transesterification of high free fatty acid oil (waste cooking oil) to biodiesel: a review, *Biotechnol. Adv.* 28 (2010) 500–518, <https://doi.org/10.1016/j.biotechadv.2010.03.002>.
- [16] W.N.N.W. Omar, N.A.S. Amin, Biodiesel production from waste cooking oil over alkaline modified zirconia catalyst, *Fuel Process. Technol.* 92 (2011) 2397–2405, <https://doi.org/10.1016/j.fuproc.2011.08.009>.
- [17] N. Pal, M. Paul, A. Bhaumik, Highly ordered Zn-doped mesoporous silica: an efficient catalyst for transesterification reaction, *J. Solid State Chem.* 184 (2011) 1805–1812, <https://doi.org/10.1016/j.jssc.2011.05.033>.
- [18] W. Xie, X. Huang, Synthesis of biodiesel from soybean oil using heterogeneous KF/ZnO catalyst, *Catal. Lett.* 107 (2006) 53–59, <https://doi.org/10.1007/s10562-005-9731-0>.
- [19] S.M. Coman, V.I. Parvulescu, Heterogeneous catalysis for biodiesel production, *Role Catal. Sustain. Prod. Bio-Fuels Bio-Chemicals* (2013) 93–136, <https://doi.org/10.1016/B978-0-444-56330-9.00004-8>.
- [20] J. Santos, J. Phillips, J.A. Dumesic, Metal-support interactions between iron and titania for catalysts prepared by thermal decomposition of iron pentacarbonyl and by impregnation, *J. Catal.* 81 (1983) 147–167, [https://doi.org/10.1016/0021-9517\(83\)90154-9](https://doi.org/10.1016/0021-9517(83)90154-9).
- [21] D.D. Bala, M. Misra, D. Chidambaram, Solid-acid catalyzed biodiesel production, part I: biodiesel synthesis from low quality feedstock, *J. Clean. Prod.* 142 (2017) 4169–4177, <https://doi.org/10.1016/j.jclepro.2016.02.128>.
- [22] C. You, C. Yu, X. Yang, Y. Li, H. Huo, Z. Wang, Y. Jiang, X. Xu, K. Lin, Double-shelled hollow mesoporous silica nanosphere as acid-base bifunctional catalyst for cascade reactions, *New J. Chem.* 42 (2018) 4095–4101, <https://doi.org/10.1039/C7NJ04670G>.
- [23] F.H. Santosa, L. Laysandra, F.E. Soetaredjo, S.P. Santoso, S. Ismadji, M. Yuliana, A facile noncatalytic methyl ester production from waste chicken tallow using single step subcritical methanol: optimization study, *Int. J. Energy Res.* 43 (2019) 8852–8863, <https://doi.org/10.1002/er.4844>.
- [24] X. Zhou, X. Cheng, W. Feng, K. Qiu, L. Chen, W. Nie, Z. Yin, X. Mo, H. Wang, C. He, Synthesis of hollow mesoporous silica nanoparticles with tunable shell thickness and pore size using amphiphilic block copolymers as core templates, *Dalton Trans.* 43 (2014) 11834–11842, <https://doi.org/10.1039/c4dt01138d>.
- [25] S. Cao, Z. Zhao, X. Jin, W. Sheng, S. Li, Y. Ge, M. Dong, W. Wu, L. Fang, Unique double-shelled hollow silica microspheres: template-guided self-assembly, tunable pore size, high thermal stability, and their application in removal of neutral red, *J. Mater. Chem.* 21 (2011) 19124–19131, <https://doi.org/10.1039/c1jm13011k>.
- [26] N.B. Klinghoffer, M.J. Castaldi, A. Nzihou, Catalyst properties and catalytic performance of char from biomass gasification, *Ind. Eng. Chem. Res.* 51 (2012) 13113–13122, <https://doi.org/10.1021/ie3014082>.
- [27] M. Zakeri, A. Samimi, M. Shafiee Afarani, A. Salehirad, Effects of porosity and pore size distribution on mechanical strength reliability of industrial-scale catalyst during preparation and catalytic test steps, *Part. Sci. Technol.* 36 (2018) 96–103, <https://doi.org/10.1080/02726351.2016.1220437>.
- [28] T. Pangestu, Y. Kurniawan, F.E. Soetaredjo, S.P. Santoso, W. Irawaty, M. Yuliana, S.B. Hartono, S. Ismadji, The synthesis of biodiesel using copper based metal-organic framework as a catalyst, *J. Environ. Chem. Eng.* 7 (2019) 103277, <https://doi.org/10.1016/j.jece.2019.103277>.
- [29] N. Rahmat, N. Sadon, M.A. Yusuf, Thermogravimetric analysis (TGA) profile at different calcination conditions for synthesis of PTES-SBA-15, *Am. J. Appl. Sci.* 14 (2017) 938–944, <https://doi.org/10.3844/ajassp.2017.938.944>.
- [30] Y.Y. Margaretha, H.S. Prastyo, A. Ayucitra, S. Ismadji, Calcium oxide from pomacea sp. shell as a catalyst for biodiesel production, *Int. J. Energy Environ. Eng.* 3 (2012) 1–9, <https://doi.org/10.1186/2251-6832-3-33>.
- [31] A.M. Dehkhoda, A.H. West, N. Ellis, Biochar based solid acid catalyst for biodiesel production, *Appl. Catal. Gen.* 382 (2010) 197–204, <https://doi.org/10.1016/j.apcata.2010.04.051>.
- [32] C. Samart, P. Sreetongkittikul, C. Sookman, Heterogeneous catalysis of transesterification of soybean oil using K1/mesoporous silica, *Fuel Process. Technol.* 90 (2009) 922–925, <https://doi.org/10.1016/j.fuproc.2009.03.017>.
- [33] G. Baskar, S. Soumiya, Production of biodiesel from castor oil using iron (II) doped zinc oxide nanocatalyst, *Renew. Energy* 98 (2016) 101–107, <https://doi.org/10.1016/j.renene.2016.02.068>.
- [34] B. Gurunathan, A. Ravi, Biodiesel production from waste cooking oil using copper doped zinc oxide nanocomposite as heterogeneous catalyst, *Bioresour. Technol.* 188 (2015) 124–127, <https://doi.org/10.1016/j.biortech.2015.01.012>.
- [35] J. Cai, Q.Y. Zhang, F.F. Wei, J.S. Huang, Y.M. Feng, H.T. Ma, Y. Zhang, Preparation of copper (II) containing phosphomolybdic acid salt as catalyst for the synthesis of biodiesel by esterification, *J. Oleo Sci.* 67 (2018) 427–432, <https://doi.org/10.5650/jos.ess17208>.
- [36] C. Samart, C. Chaiya, P. Reubroycharoen, Biodiesel production by methanolysis of soybean oil using calcium supported on mesoporous silica catalyst, *Energy Convers. Manag.* 51 (2010) 1428–1431, <https://doi.org/10.1016/j.enconman.2010.01.017>.
- [37] W. Xie, H. Li, Alumina-supported potassium iodide as a heterogeneous catalyst for biodiesel production from soybean oil, *J. Mol. Catal. Chem.* 255 (2006) 1–9, <https://doi.org/10.1016/j.molcata.2006.03.061>.
- [38] M. Farooq, A. Ramli, Biodiesel production from low FFA waste cooking oil using heterogeneous catalyst derived from chicken bones, *Renew. Energy* 76 (2015) 362–368, <https://doi.org/10.1016/j.renene.2014.11.042>.
- [39] R. Alenezi, G.A. Leeke, J.M. Winterbottom, R.C.D. Santos, A.R. Khan, Esterification kinetics of free fatty acids with supercritical methanol for biodiesel production, *Energy Convers. Manag.* 51 (2010) 1055–1059, <https://doi.org/10.1016/j.enconman.2009.12.009>.
- [40] M. Farooq, A. Ramli, D. Subbarao, Biodiesel production from waste cooking oil using bifunctional heterogeneous solid catalysts, *J. Clean. Prod.* 59 (2013) 131–140, <https://doi.org/10.1016/j.jclepro.2013.06.015>.
- [41] I. Amalia Kartika, M. Yani, D. Ariono, P. Evon, L. Rigal, Biodiesel production from *Jatropha* seeds: solvent extraction and in situ transesterification in a single step, *Fuel* 106 (2013) 111–117, <https://doi.org/10.1016/j.fuel.2013.01.021>.
- [42] Z. Wei, C. Xu, B. Li, Application of waste eggshell as low-cost solid catalyst for biodiesel production, *Bioresour. Technol.* 100 (2009) 2883–2885, <https://doi.org/10.1016/j.biortech.2008.12.039>.
- [43] A. Demirbas, Biodiesel from waste cooking oil via base-catalytic and supercritical methanol transesterification, *Energy Convers. Manag.* 50 (2009) 923–927, <https://doi.org/10.1016/j.enconman.2008.12.023>.
- [44] I.A. Reşitoğlu, A. Keskin, M. Gürü, The optimization of the esterification reaction in biodiesel production from trap grease, *Energy Sources, Part A Recover. Util. Environ. Eff.* 34 (2012) 1238–1248, <https://doi.org/10.1080/15567031003792395>.
- [45] A. Hayyan, F.S. Mjalli, M.A. Hashim, M. Hayyan, I.M. AlNashef, S.M. Al-Zahrani, M.A. Al-Saadi, Ethanesulfonic acid-based esterification of industrial acidic crude palm oil for biodiesel production, *Bioresour. Technol.* 102 (2011) 9564–9570, <https://doi.org/10.1016/j.biortech.2011.07.074>.
- [46] S.L. Lee, Y.C. Wong, Y.P. Tan, S.Y. Yew, Transesterification of palm oil to biodiesel by using waste obtuse horn shell-derived CaO catalyst, *Energy Convers. Manag.* 93 (2015) 282–288, <https://doi.org/10.1016/j.enconman.2014.12.067>.
- [47] W. Xie, T. Wang, Biodiesel production from soybean oil transesterification using tin oxide-supported WO₃ catalysts, *Fuel Process. Technol.* 109 (2013) 150–155, <https://doi.org/10.1016/j.fuproc.2012.09.053>.
- [48] M. Kouzu, J.S. Hidaka, Transesterification of vegetable oil into biodiesel catalyzed by CaO: a review, *Fuel* 93 (2012) 1–12, <https://doi.org/10.1016/j.fuel.2011.09.015>.
- [49] D.M. Marinković, M.V. Stanković, A.V. Veličković, J.M. Avramović, M.R. Miladinović, O.O. Stamenković, V.B. Veljković, D.M. Jovanović, Calcium oxide as a promising heterogeneous catalyst for biodiesel production: current state and perspectives, *Renew. Sustain. Energy Rev.* 56 (2016) 1387–1408, <https://doi.org/10.1016/j.rser.2015.12.007>.
- [50] A.K. Endalew, Y. Kiros, R. Zanzi, Inorganic heterogeneous catalysts for biodiesel production from vegetable oils, *Biomass Bioenergy* 35 (2011) 3787–3809, <https://doi.org/10.1016/j.biombioe.2011.06.011>.